Journal of the Australian Ceramic Society (2023) 59:1095–1109
https://doi.org/10.1007/s41779-023-00900-z

RESEARCH

On tungsten barium phosphate glasses: Elastic moduli, gamma-ray shielding properties as well as transmission factor (TF)

Norah A. M. Alsaif[1] · Duygu Sen Baykal[2] · Wiam Elshami[3] · Hesham M. H. Zakaly[4,5] · Shams A. M. Issa[5,6] · Antoaneta Ene[7] · Y. S. Rammah[8]

Received: 6 November 2022 / Revised: 21 March 2023 / Accepted: 14 May 2023 / Published online: 30 May 2023

Abstract

Moduli of elasticity and the ability of gamma radiation shielding as well as transmission factor (TF) of four samples of tungsten bario-phosphate glasses with chemical formula $xBaO\text{-}40WO_3\text{-}(60\text{-}x)P_2O_5$: (x = 10, 20, 30, and 40 mol% glasses) have been examined. The glass samples have been coded as S1: $10BaO\text{-}40WO_3\text{-}50P_2O_5$, S2: $20BaO\text{-}40WO_3\text{-}40P_2O_5$, S3: $30BaO\text{-}40WO_3\text{-}30P_2O_5$, and S4: $40BaO\text{-}40WO_3\text{-}20P_2O_5$. Makishima-Mackenzie model, the newly online Phy-X/PSD software, and Monte Carlo code were applied to achieve the mentioned purposes. The total dissociation energy (G_t) values were decreased from 62.58 (kJ/cm^3) for S1 glasses to 55.92 (kJ/cm^3) for S4 glasses. The total packing density (V_t) was 0.613, 0.626, 0.612, and 0.643, for S1, S2, S3, and S4, respectively. Values of Young's (E^{MM}) modulus were 76.759 GPa, 75.631 GPa, 71.167 GPa, and 71.966 GPa and Poisson's ratio (σ^{MM}) possessed the values 0.273 GPa, 0.278 GPa, 0.273 GPa, and 0.284 GPa for S1, S2, S3, and S4, respectively. The S4 sample possessed the highest values of both linear (μ) and mass (μ_m) attenuation coefficients. However, $(\mu, \mu_m)_{S1} < (\mu, \mu_m)_{S2} < (\mu, \mu_m)_{S3} < (\mu, \mu_m)_{S4}$. Also, The S4 sample possessed the lowest values of half value layer (HVL), tenth (TVL) value layers, and mean free path (MFP) among all studied glasses. Therefore, $(HVL, TVL, MFP)_{S4} < (HVL, TVL, MFP)_{S3} < (HVL, TVL, MFP)_{S2} < (HVL, TVL, MFP)_{S1}$. Both effective atomic number (Z_{eff}) and electron density (N_{eff}) of the investigated glasses have as similar trend. In terms of transmission factor (TF), the sample S4 achieved the minimum values at a thickness of 3 cm. However, the S4 sample exhibited superior radiation shielding characteristics.

Keywords Glasses · Moduli of elasticity · Phy-X/PSD · Radiation shielding · MCNPX

Introduction

Aside from the benefits of ionizing radiation, concerns about the quantity of radiation generated and absorbed during the usage of radiation were noted. The biological risks of radiation were reported following the discovery of X-ray [1]. Increased risk of cancer is also associated with radiation exposure. Studies found an increased risk of cancer among radiation workers [2] and a significant association between radiation exposure and mortality [3].

✉ Y. S. Rammah
dr_yasser1974@yahoo.com

1 Department of Physics, College of Science, Princess Nourah Bint Abdulrahman University, P.O. Box 84428, Riyadh 11671, Saudi Arabia

2 Vocational School of Health Sciences, Medical Imaging Techniques, Istanbul Kent University, Istanbul 34433, Turkey

3 Department of Medical Diagnostic Imaging, College of Health Sciences, University of Sharjah, 27272 Sharjah, United Arab Emirates

4 Institute of Physics and Technology, Ural Federal University, 620002 Ekaterinburg, Russia

5 Physics Department, Faculty of Science, Al-Azhar University, Assiut 71524, Egypt

6 Physics Department, Faculty of Science, University of Tabuk, Tabuk 47512, Saudi Arabia

7 INPOLDE Research Center, Department of Chemistry, Physics and Environment, Faculty of Sciences and Environment, Dunarea de Jos University of Galati, 47 Domneasca Street, 800008 Galati, Romania

8 Department of Physics, Faculty of Science, Menoufia University, Shebin El-Koom 32511, Menoufia, Egypt

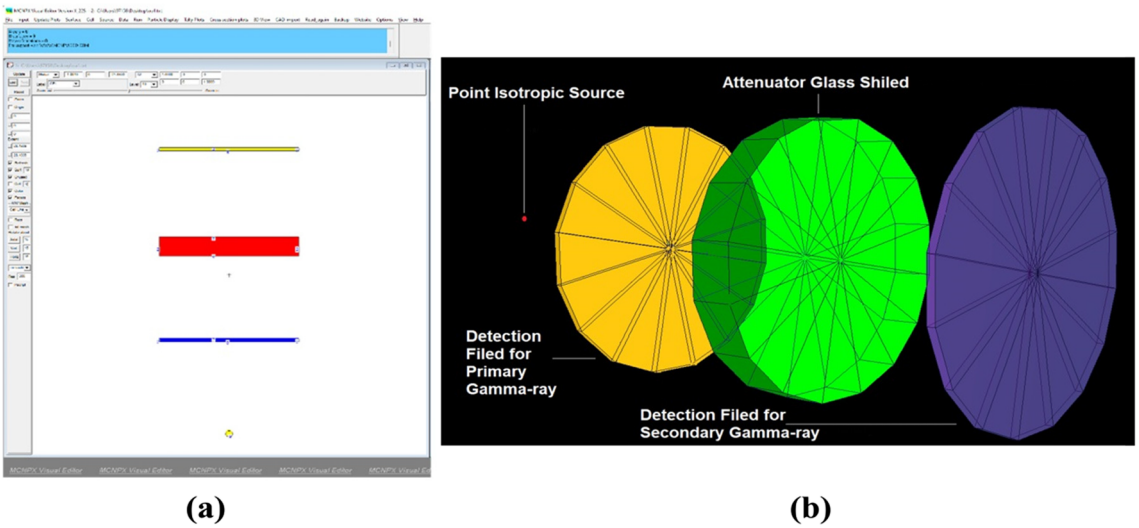

Fig. 1 **(a)** 2-D view of designed MCNPX simulation setup **(b)** 3-D illustration of designed MCNPX setup (2-D and 3-D views are obtained from MCNPX Visual Editor VisedX22S)

Therefore, radiation facilities must ensure that radiation safety procedures and practices are properly implemented to support safe practice [4]. Protection from radiation, which poses a hazard to human health, is a fascinating scientific research area. With decreasing radiation exposure time and increasing distance from the radiation source, radiation shielding is one of the cornerstones of radiation protection. Radiation shields act as barriers and protect from penetrating radiation such as gamma rays and neutrons [5–11]. Radiation shielding is commonly used to protect medical patients and radiation workers from direct and secondary radiation. Shielding has a significant role in reducing radiation dose to patients. Nevertheless, the use of shielding is applied to other industries applied radiation in practices such as research, nuclear energy, and defense [12]. The majority of currently available shielding materials are made of lead (Pb) and have a number of drawbacks, including weight, strength, and the lack of transparent glass [13, 14]. Researchers are working hard to develop better, next-generation shielding materials that are also ecologically beneficial. Therefore, additive and alternative materials are to be examined to increase visibility, cost, weight, and ease of production. For this reason, many materials such as glasses, metals, and composites have been tested to improve the efficiency of shielding materials [15–24]. As mentioned above, nowadays the glass materials are used in several nuclear radiation facilities. Many of researchers studied the effectiveness of glass as the radiation shielding materials such as: Na_2O_5-Al_2O_3-SiO_2-CaO-WO_3 glass [25], $Li_2B_4O_7$ glass [26], TeO_2–Ta_2O_5-Bi_2O_3 glass [27], BaO-MgO-Na_2O-Al_2O_3-B_2O_3 glass [28], WO_3 doped TeO_2–B_2O_3 glass [29], TeO_2–ZnO–NaF–LiF glass system [30], BaO-TeO_2-Cr_2O_3-B_2O_3 glass system [31], and Na_2O-$BaCl_2$-B_2O_3-BCD glass [32]. However, a research in which a gamma-ray energy range in a very wide spectrum was not found on existing glass samples. More importantly, the TF factor calculations performed in addition to the photon energy in this broad range also raised the level of the characterization process, providing a better understanding of both the particular shielding parameters and all the absorption characteristics of the glass samples. As previously, due to glasses have several interesting physical and chemical properties such as transparency, ease in preparation, low cost, have good optical, thermal, mechanical, and electrical properties, they can applied in various industrial and medical applications [20, 33–36]. Therefore, recently several authors paid their efforts to design and prepare new promising glasses for optical and radiation shielding applications [20–24].

The primary objective of the current work is to examine how barium oxide (BaO) affects the ability of tungsten bario-phosphate (WO_3/ BaO/P_2O_5) glass to shield radiation and mechanical forces. The conclusions may help with a better knowledge of radiation safety concepts for the examined glasses and their versatility in use.

Table 1 Packing density factor (V_i), and dissociation/bond energy per unit volume (G_i) of the oxides BaO, WO_3, and P_2O_5

Oxide	V_i (cm^3/mol)	G_i (kJ/cm^3)
BaO	13.1	40.6
WO_3	21.3	67.8
P_2O_5	34.8	62.8

Table 2 Total ionic packing density (V_t), total dissociation energy (G_t), Young's modulus (E^{MM}), bulk modulus (K^{MM}), shear modulus (S^{MM}), longitudinal modulus (L^{MM}) and Poisson's ratio (σ^{MM}) based on Makishima-Mackenzie model of the studied glasses. The x_i is mole fraction of the component i of an oxide glass and V_m is the molar volume of the glass samples

Parameters and elastic moduli	V_t	G_t (kJ/cm^3)	E^{MM}(GPa)	K^{MM}(GPa)	S^{MM}(Gpa)	L^{MM}(Gpa)	σ^{MM}(GPa)
S1	0.613	62.58	76.759	56.490	30.136	96.571	0.273
S2	0.626	60.36	75.631	56.859	29.582	96.204	0.278
S3	0.6120	58.14	71.167	52.267	27.950	89.442	0.273
S4	0.643	55.92	71.966	55.570	28.020	92.838	0.284

Materials and methods

Tungsten bario-phosphate glasses

Four samples of tungsten bario-phosphate glasses with chemical composition xBaO-40WO_3-(60-x)P_2O_5: (x = 10, 20, 30, and 40 mol%) were selected from previous work [37]. Some details of the studied glasses as the following:

S1: 10BaO-40WO_3-50P_2O_5
S2: 20BaO-40WO_3-40P_2O_5
S3: 30BaO-40WO_3-30P_2O_5
S4: 40BaO-40WO_3-20P_2O_5

Mechanical features of tungsten bario-phosphate glasses

Makishima-Mackenzie [38–42] was used to calculate the elastic moduli and Poisson's ratio of the tungsten bario-phosphate glasses (S1-S4) that were investigated. The elastic moduli are known to be a function of the packing density (V_t) and the dissociation energy (G_t) per unit volume of the chemical-bonds in the glass, as [38–42]:

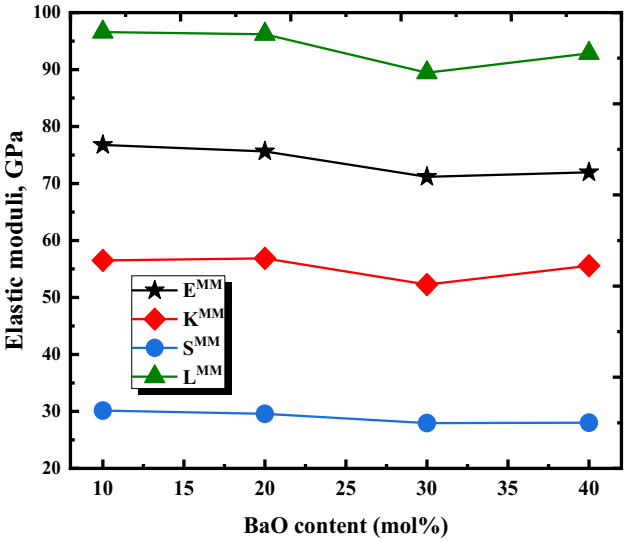

Fig. 3 Variation of elastic moduli as a function of BaO content mol% of the investigated glasses

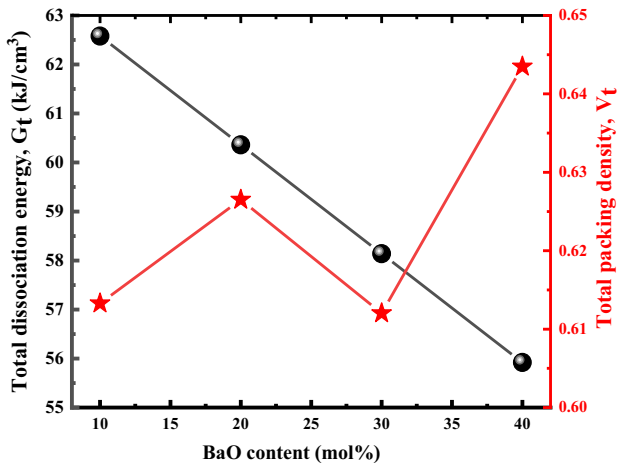

Fig. 2 Variation of G_t and V_t as a function of BaO content (mol%) of the investigated glasses

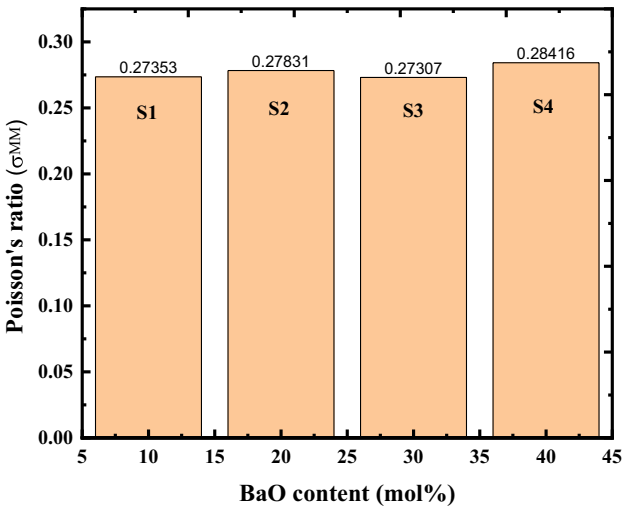

Fig. 4 Variation of Poisson's ratio as a function of BaO content (mol%) of the investigated glasses

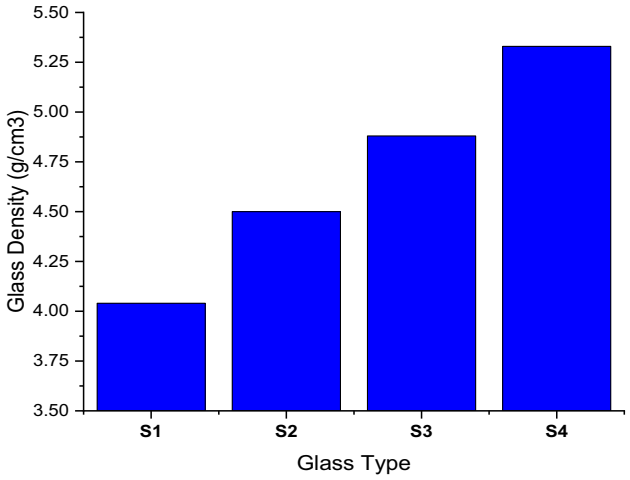

Fig. 5 Describes differences among densities of glass types

$$V_t = \left(\frac{1}{V_m}\right)\sum_i (V_i x_i) \tag{1}$$

$$G_t = \sum_i (G_i x_i)\ \ (\mathrm{kJ}/cm^3) \tag{2}$$

where V_i is the ionic radius and G_i is the average strength of each oxide

The Young`s (E^{MM}), bulk (K^{MM}), shear (S^{MM}), and longitudinal (L^{MM}) moduli may be calculated in GPa unit through the following Eqs. (3–6) [38–42]:

$$E^{MM} = 2V_t G_t \tag{3}$$

$$K^{MM} = 1.2V_t E^{MM} \tag{4}$$

$$S^{MM} = \frac{(3E^{MM}K^{MM})}{(9K^{MM} - E^{MM})} \tag{5}$$

$$L^{MM} = K^{MM} + \frac{4}{3}S^{MM} \tag{6}$$

Poisson's ratio (σ_{MM}) can be given as

$$\sigma^{MM} = \left(\frac{E^{MM}}{2G^{MM}}\right) - 1 \tag{7}$$

Radiation shielding parameters and transmission factors (TFs)

It is well understood that the photon attenuation efficiency of substances may be affected by changes in their composition. Such modifications may be evaluated in several ways, including by analyzing parameters or by computing an evaluation of the whole content. TF [43] is the quantitative percentage (%) of the incident radiation's intensity to the secondary radiation intensity after attenuation inside the glass shiled. For several common radioisotope energies, TFs and gamma-ray attenuation properties of the explored glasses were quantified using a general-purpose Monte Carlo simulation software, MCNPX (Version 2.7.0) [44]. Moreover, Phy-X/PSD [45] program was employed in terms of determining the fundamental gamma-ray shielding parameters. Graphical representations of the MCNPX simulation structure from two and

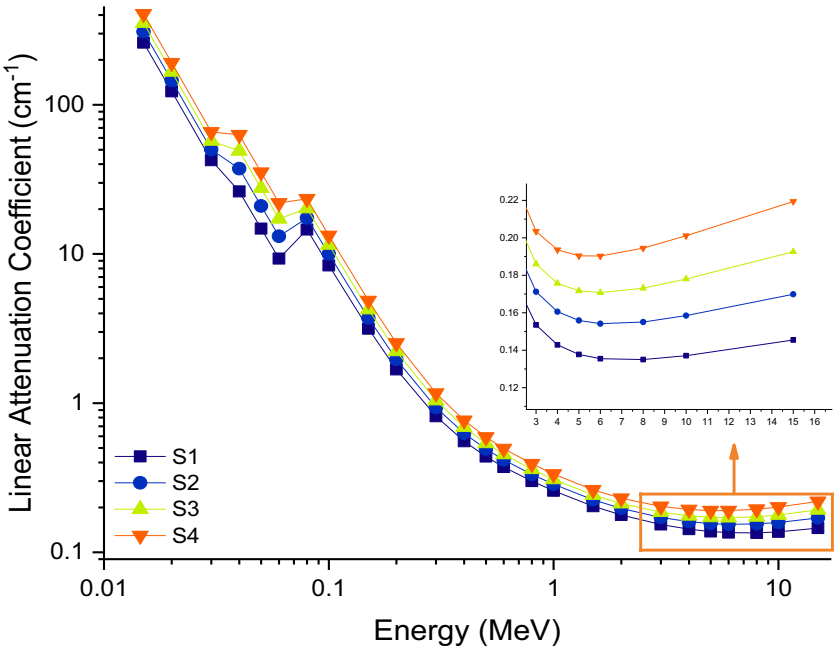

Fig. 6 Variations of linear attenuation coefficient (cm^{-1}) with photon energy (MeV) for all S1-S4 glasses

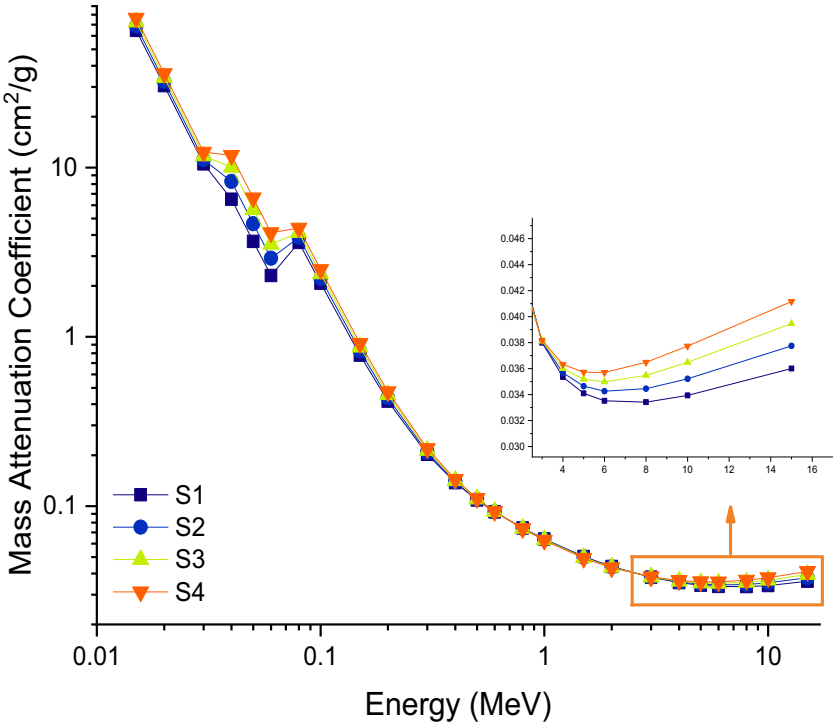

Fig. 7 Variations of mass attenuation coefficients (cm^2/g) with photon energy (MeV) for all S1-S4 glasses

three-dimensional perspectives, respectively, are shown in Fig. 1a and b. These images are utilized to compute the gamma-ray transmission factor (TF) values of the glass shields under investigation. The first step of any Monte Carlo simulation software is the formation of an appropriate input file. This file should include all the components that will make up the simulation platform on which the research will be carried out. Throughout every step of this investigation, a straightforward input file was constructed to provide information on the cells, surfaces, and data cards. This file was afterwards presented in the manner that is seen in Fig. 1. The percentage distributions and densities of the elements were provided for each specimen are the two key determinants that may be found in the

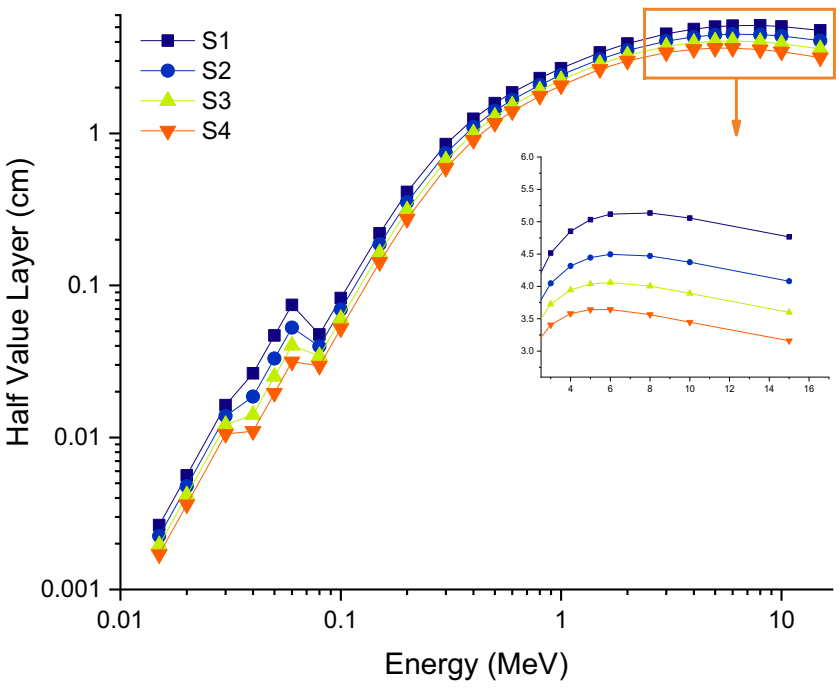

Fig. 8 Variations of half value layer (cm) with photon energy (MeV) for all S1-S4 glasses

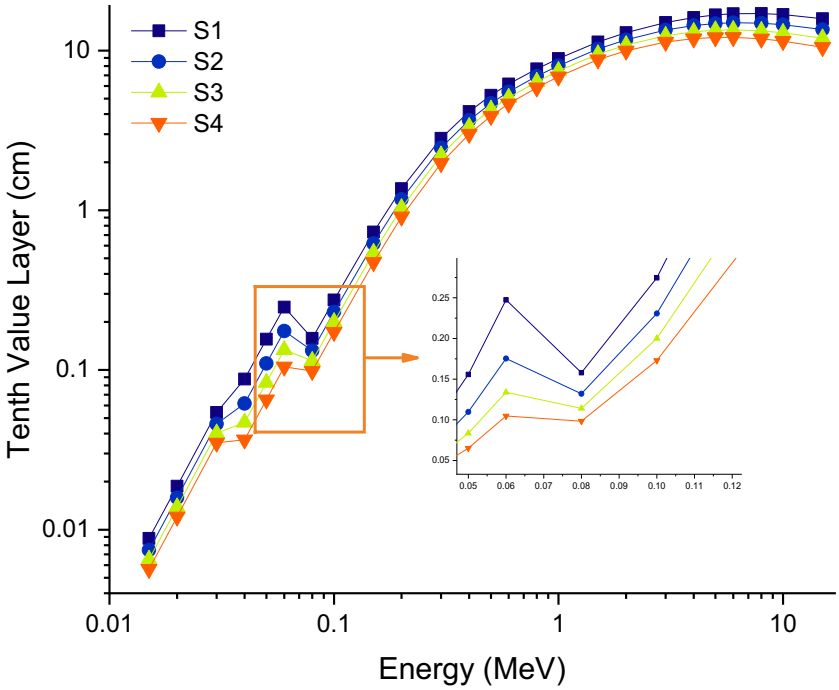

Fig. 9 Variations of tenth value layer (cm) with photon energy (MeV) for all S1-S4 glasses

input file that was produced consequently. The results of this investigation will be explained in the sections that follow. Throughout the stages of the Monte Carlo simulation, we relied on a primary processor that was comprised of a Lenovo® Think-Station-P620/30E0008QUS Workstation. In the meanwhile, it was discovered that the total relative error rate for the process of simulation was less than 1%.

Results and discussions

Mechanical characteristics

Values of V_i and G_i of P_2O_5, WO_3, and BaO oxides are collected in Table 1. Table 2 contains the obtained values for V_t and G_t. Figure 2 shows how G_t and V_t change as a function of

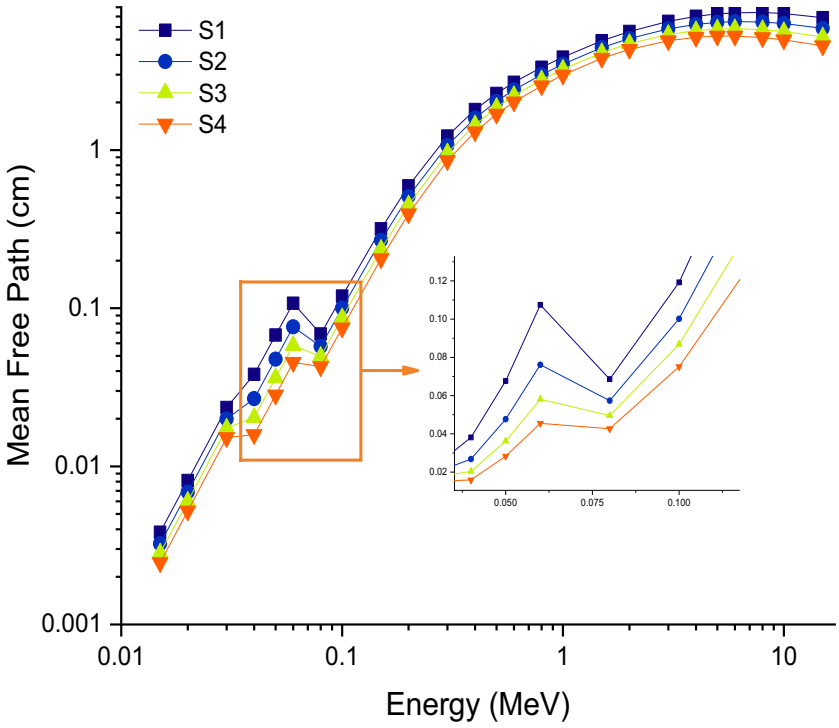

Fig. 10 Variations of mean free path (cm) with photon energy (MeV) for all S1-S4 glasses

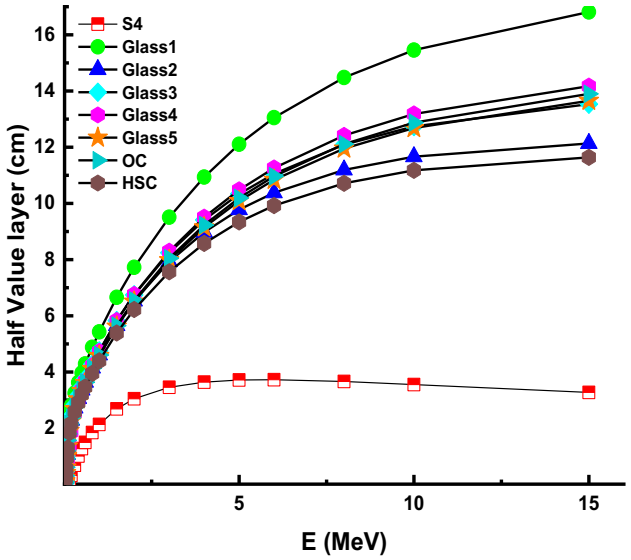

Fig. 11 Variations of half value layer (cm) with photon energy (MeV) for S4 glass comparing to different glasses and concrete

the amount of barium oxide (BaO) in mol% of S1-S4 glasses. For S1, S2, S3, and S4, the (Vi) was 0.613, 0.626, 0.612, and 0.643, respectively. This pattern might be explained by the fact that BaO has an ionic radius that is lower than P_2O_5. As shown in Fig. 2, the Gt values fell from 62.58 (kJ/cm^3) for S1 glasses to 55.92 (kJ/cm^3) for S4 glasses. The trend of the (G_t) is due to the P_2O_5 has dissociation energy (62.8 kJ/cm^3) higher compared to that of BaO (40.6 kJ/cm^3). Relation (3) used to calculate the Young`s elastic (E^{MM}) modulus by substituting for (V_t) and (G_t) values. The obtained values of the (E^{MM}) are collected in Table 2 and depicted in Fig. 3. The (E^{MM}) values are 76.759 GPa, 75.631 GPa, 71.167 GPa, and 71.966 GPa, respectively. The reduction of the (E^{MM}) can be attributed to the decrease of the G_t with increasing of BaO concentration. Applying relation (4), values of the bulk (K^{MM}) modulus of S1-S4 samples were given and collected in Table 2. Values of the (K^{MM}) were 56.490 GPa, 56.859 GPa, 52.267 GPa, and 55.570 GPa, respectively. Both shear (S^{MM}) and longitudinal (L^{MM}) elastic moduli were computed, collected in Table 2, and drawn in Fig. 3. Values of the (S^{MM}) were 30.136 GPa, 29.582 GPa, 27,950 GPa, and 28.020 GPa, while values of the (L^{MM}) were 96.571 GPa, 96.204 GPa, 89.442 GPa, 92.838 GPa, for S1, S2, S3, and S4 glasses, respectively. Poisson's ratio (σ^{MM}) of the investigated glasses was examined via relation (7). As in Table 2 and Fig. 4, the values of (σ^{MM}) were 0.273 GPa, 0.278 GPa, 0.273 GPa, and 0.284 GPa for S1, S2, S3, and S4, respectively.

Gamma-ray shielding properties of tungsten bario-phosphate glasses

The purpose of this research is to investigate novel glasses derived from the system tungsten bario-phosphate glasses ($BaO\text{-}P_2O_5\text{-}WO_3$). The preparation and investigation will concentrate on the fundamental physical characteristics of these glasses as a consequence of their

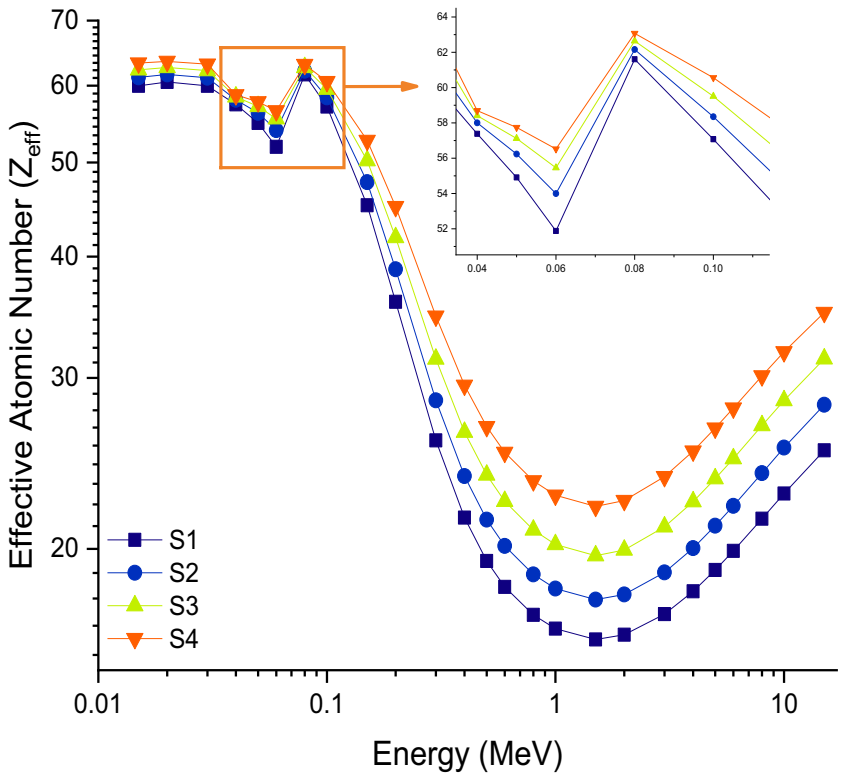

Fig. 12 Variations of effective atomic number (Z_{eff}) with photon energy (MeV) for all S1-S4 glasses

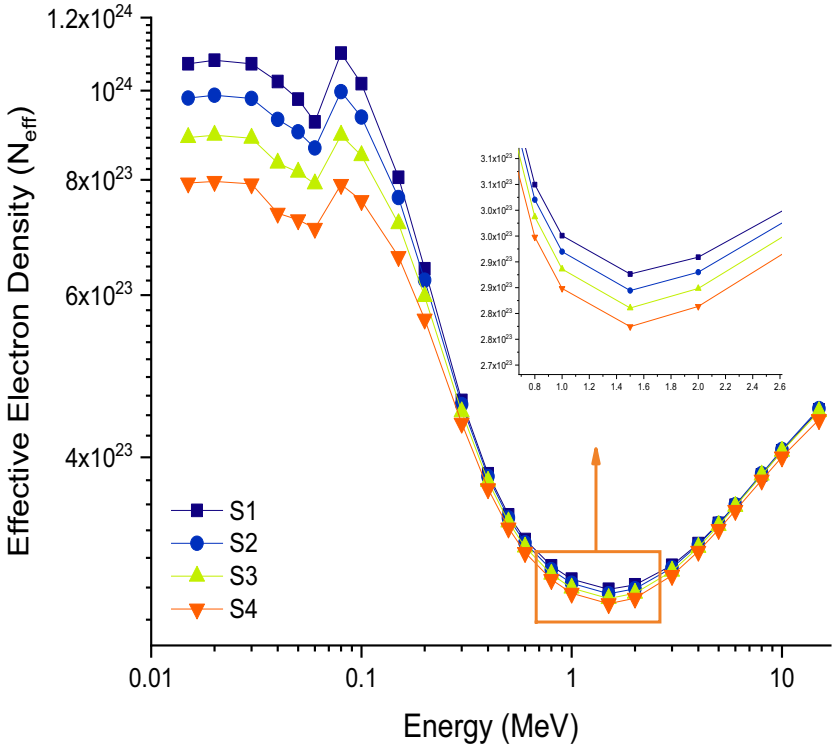

Fig. 13 Variations of effective electron density (electrons/g) with photon energy (MeV) for all S1-S4 glasses

chemical configurations. The glass samples' densities ranged between 4.04 to 5.33 g.cm^{-3}, as S1 has the lowest density and S4 the highest, presented in Fig. 5. The variations of (μ) and (μ_m) of glasses S1-S4 with photon energy (MeV) are demonstrated in Figs. 6 and 7. Both figures exhibit nearly identical pattern of trends, as they start with a gradual decrease in S1-S4 values as photon energy increases until 0.03 MeV a sudden rise in values is detected as it is followed by the same previous behavior of gradual decrease, at 0.06 MeV another rise in values is depicted, followed by a subsequent drop in values, maintaining the same pattern in which S4 holds the highest values, followed by S3, S2 and S1 which is the lowest in numerical values among glasses. Mass attenuation coefficient (μ_m) graph (see Fig. 7) depicts closer values, almost identical at some recorded photon energy points (MeV). Photon-matter interactions in different energy zones, such as the photoelectric effect and Compton scattering, may be ascribed to the vast range of values for (μ) and (μ_m), respectively. This may be done so in order to explain the large range of values for (μ) and (μ_m). The density of a material is taken into consideration while determining the linear attenuation coefficient of a substance, in contrast to the (μ_m). According to the findings of our study, the (μ) and (μ_m) of the S4 sample were the highest across the board for all of photons energies. Calculating the half value layer, also known as the HVL, is required in order to evaluate how effective a shielding material is against the radiation that is being used. Both HVL and TVL which employ absorber materials of varying thicknesses are two distinct approaches of lowering the intensity of radiation beams. Both of these approaches are known as HVL. The HVL refers to the minimum thickness of a material that must be used in order to attenuate X-ray or gamma-ray radiation to fifty percent of its initial value. A moving

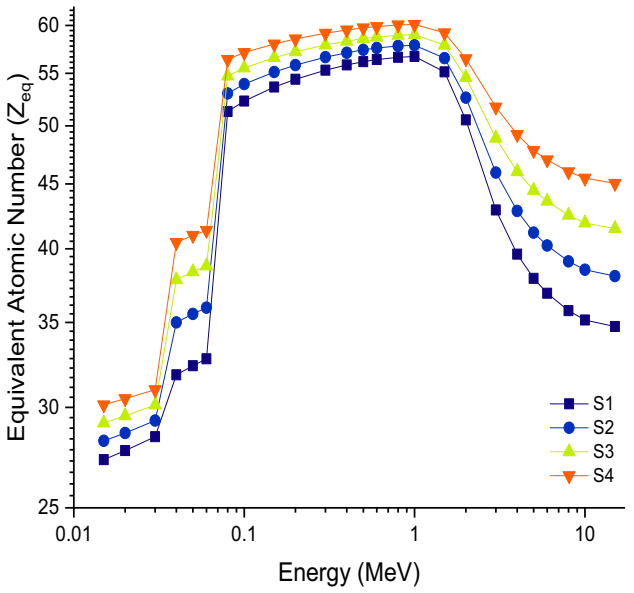

Fig. 14 Variations of equivalent atomic number (Z_{eq}) with photon energy (MeV) for all S1-S4 glasses

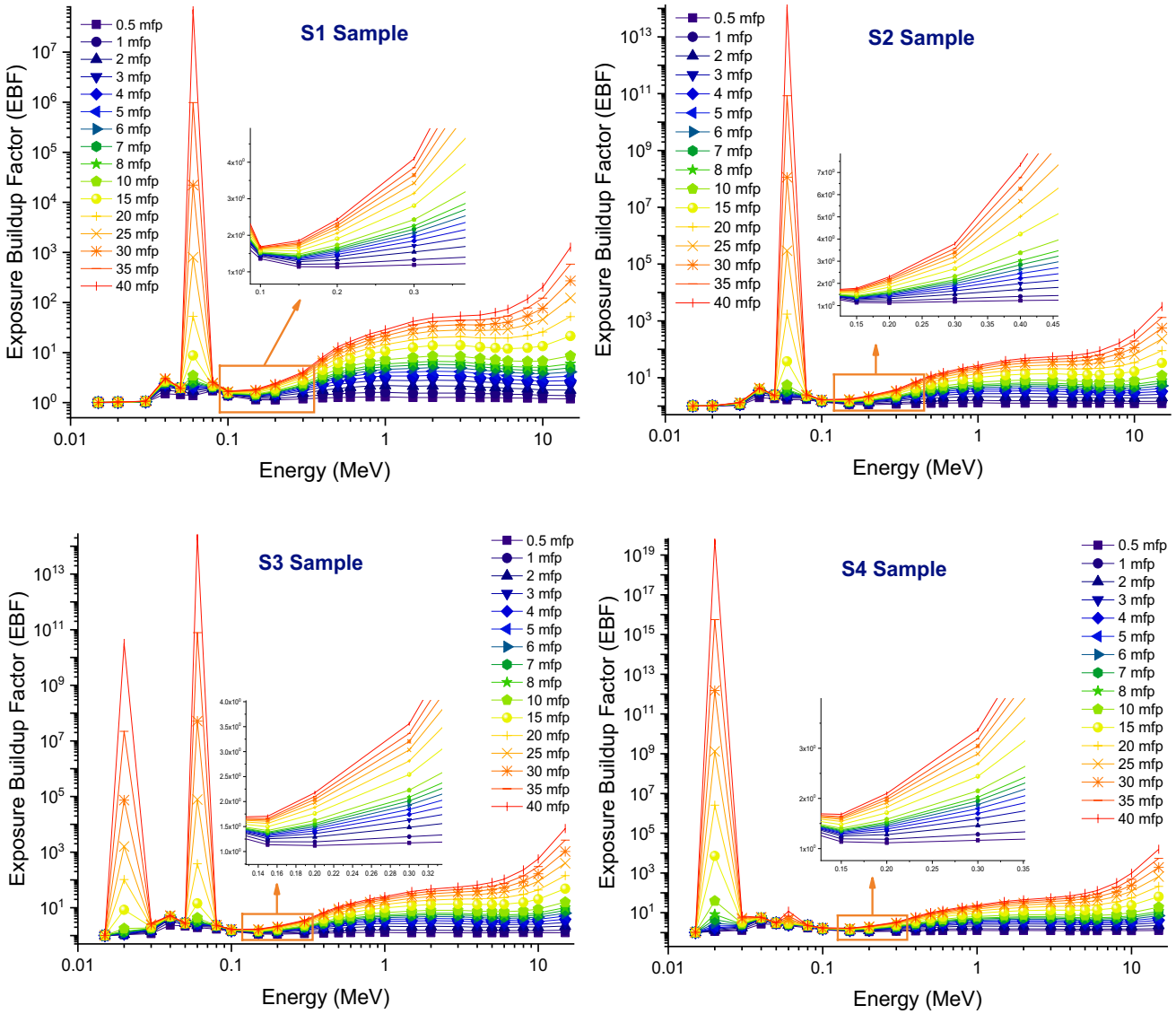

Fig. 15 Variation of exposure buildup factors (EBF) of investigated glasses at different mean free path values

particle's mean free path is the average distance it travels between subsequent collisions or impacts; this distance is referred to as the mean free path (MFP).

Figures 8, 9, and 10 depict the variations of HVL,TVL, and MFP, respectively with photon energy (MeV), these three graphs illustrate an identical trend pattern, as the three of them start with a gradual increase in values proportional to photon energy until 0.06 MeV a slight sudden drop in values occurs, after that the trend returns to its previous state of subsequent rising in values while S1-S4 values maintain the same order throughout the three trends, S1 ranks highest values, followed by S2, S3 and S4 is the lowest among four glasses. HVL and TVL values may be enhanced by using the S4 sample, which lowers gamma-ray intensity at the thinnest material thicknesses. Because of its high gamma-ray absorption rate, the mean free path (MFP) between two subsequent interactions in S4 sample is the shortest among the glasses evaluated.

Figure 11 shows the variations of HVL with photon energy for S4 glass sample comparing to glass1 [46], glass2 [47], glass3 [48], glass 4 [49], glass5 [50], ordinary concrete (OC) [51], and hematite-serpentine concrete (HSC) [51]. As shown in this figure, along selected photon energy, the S4 glass sample (this work) has the smallest HVL values.

It is inversely related to the incoming photon energy (MeV) to the effective atomic number (Z_{eff}) and the effective electron density (N_{eff}). As both graphs depict similar type of trend when seen at first glance, both trends start with a subsequent drop in values as energy (MeV) rises up to 0.06 MeV a sharp increase is noted. Then, the trend continues to descend with energy

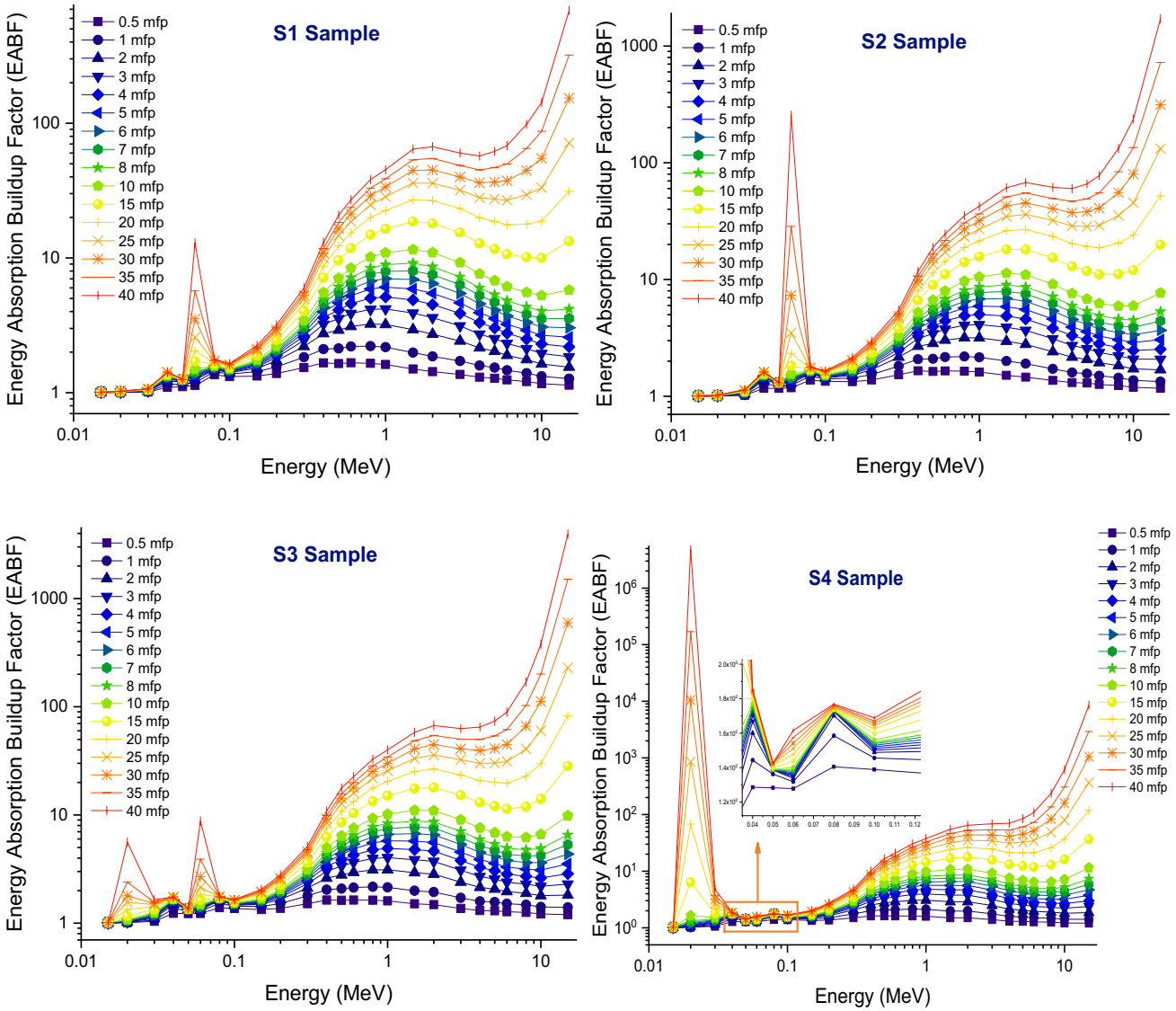

Fig. 16 Variation of energy absorption buildup factors (EABF) of investigated glasses at different mean free path values

rising up to 3 MeV values begin to increase gradually. Main differences between these two trends, in Z_{eff} (see Fig. 12), which starts with slight difference among S1-S4 values but after first sharp increase at 0.06 MeV, values diverge and start to depict more significant differences while maintaining to keep S4 as the highest value among glasses throughout the trend, followed by S3, S2 and S1 the least in value. For Fig. 13, trend starts with divergent values that illustrate noticeable numerical differences among S1-S4 then after the first sharp increase, values take part in coming closer with much less numerical difference. Throughout the trend, S1 has maintained the highest value across glasses, with S2, S3, and S4 having the lowest value. Figure 14 demonstrates the relationship between equivalent atomic number (Z_{eq}) and photon energy (MeV), as seen, trend starts with an ascending behavior with two events of sharp rising in values at 0.03 MeV and 0.06 MeV, it reaches a maximum peak at 1 MeV recording values between 56.71 and 60.10 for S1-S4 glasses, noting that S4 ranks highest values followed by S3, S2 and S1. After reaching the peak, values drop gradually.

The EBF and EABF values of the investigated glasses are presented in Figs. 15 and 16 as a function of energy (MeV) for the different mean free paths (i.e., from 0.5 to 40). When the photon's energy increases, there is a noticeable increase in these values at energies of 0.02 MeV, 0.04 MeV, 0.06 MeV, and 2 MeV. EBF and EABF variations are less evident at lower penetration depths up to 15 MeV energy, but they substantially rise

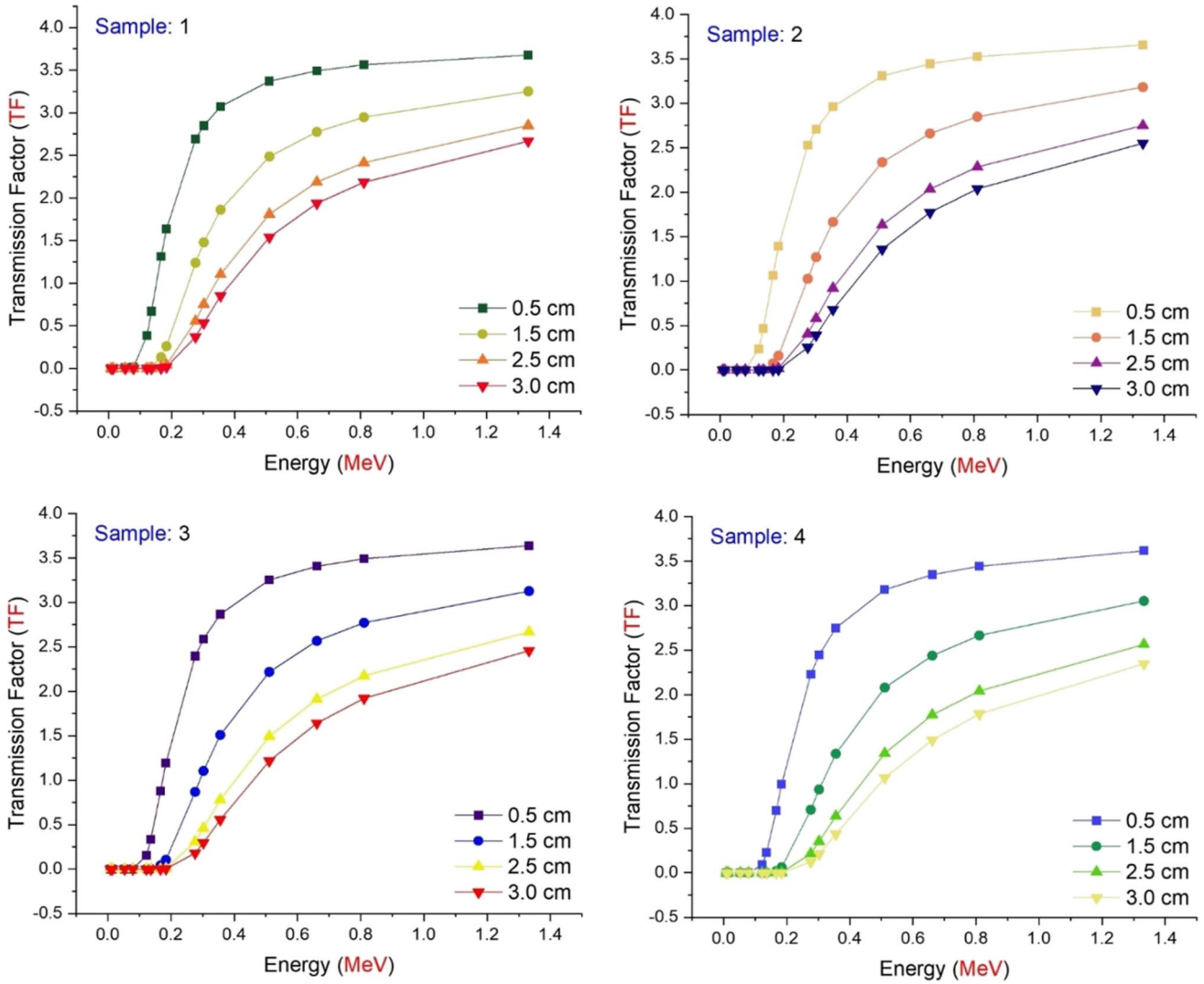

Fig. 17 Transmission factors (TFs) of investigated glasses as a function of used radioisotope energy (MeV) at different glass thicknesses

as mfp increases with energy intensities up to 15 MeV. This is because EBF and EABF fluctuations are proportional to the energy strength. It is more likely for photon build-up to occur when the mfp values are higher, especially for thicker materials and when there is a larger spectrum of incoming X-rays or gamma-rays. In addition, when it came to the fundamental gamma-ray shielding capabilities, we found that the S4 sample had the highest attenuation out of the four different glasses that were investigated.

Gamma-ray transmission factors (TFs)

The transmission factors (TFs) of the glasses that were tested are shown in Fig. 16 as a function of the radioisotope energy that was employed (MeV) at various glass thicknesses. TFs were calculated for all the glasses in two phases. In the first phase, the TFs were calculated of each glass samples for different thicknesses such as 0.5, 1.5, 2.5, and 3 cm as a function of radioisotope energies. As seen in Fig. 17, all glass samples have low TF values when gamma energies are low. However, this behavioral condition was quantified differently in relation to the TF values for various glass thicknesses. For example, at the thinnest glass thickness of 0.5 cm, all glasses had the greatest TF value, indicating that they were capable of resisting primary gamma-ray penetration to a great degree yet, as the glass thickness increased, the intensity of the transmitted primary gamma ray reduced, and the majority of the transmitted primary gamma rays were absorbed in the sample with the greatest glass thickness. This may be explained by the beneficial effect on shielding qualities of increasing the thickness of the same type of shielding material. Following observations of the glasses' behavior as a function of thickness, the second phase investigation compared four glass samples at four different thicknesses. Figure 18 shows

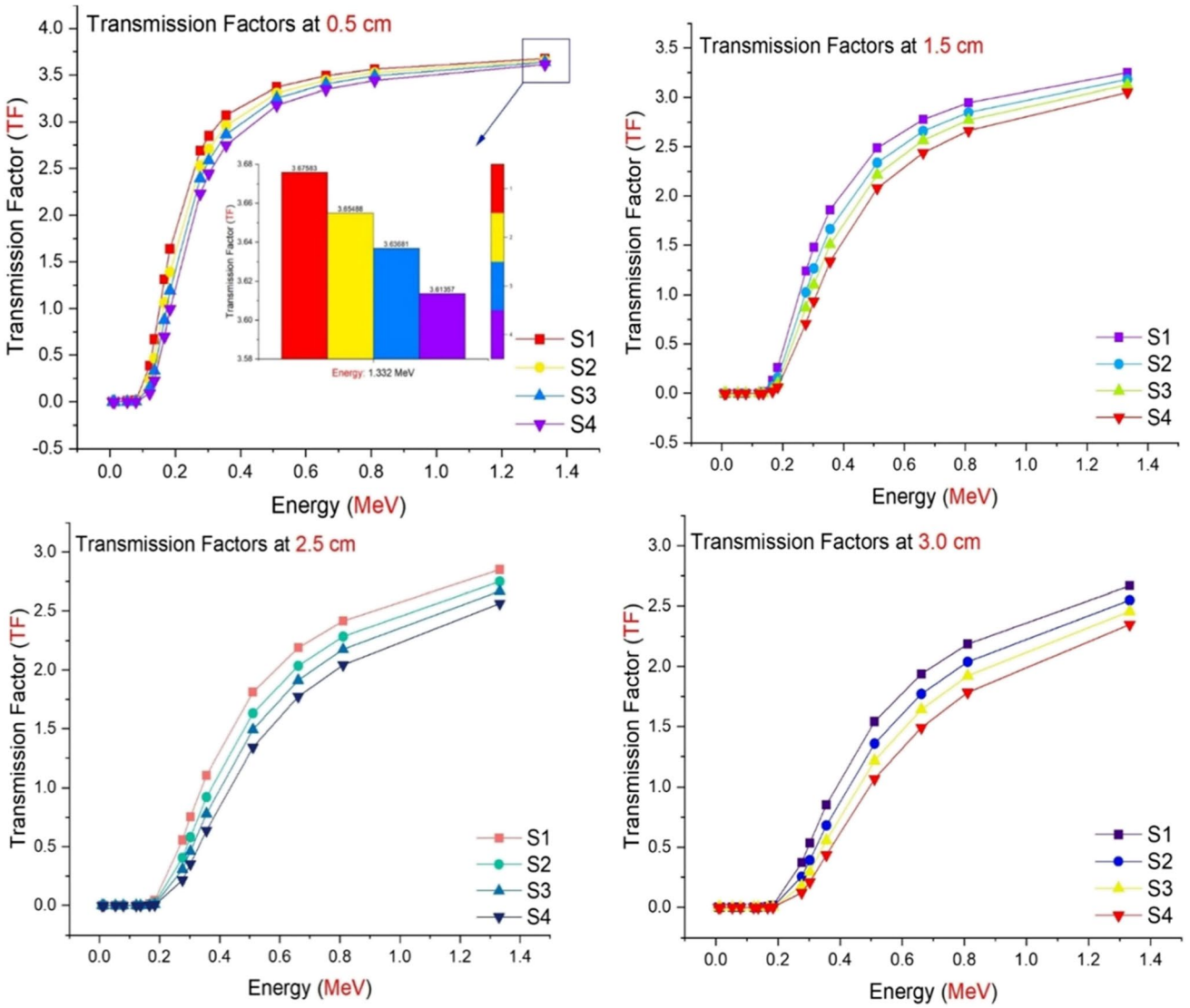

Fig. 18 Comparison of the transmission factors (TFs) as a function of used radioisotope energy (MeV) for different glass thicknesses

a comparison of the transmission factors (TFs) for various glass thicknesses as a function of the radioisotope energy that was employed (MeV). The S4 sample has the lowest gamma-ray ratios that are permitted for each thickness value that was analyzed, making its TF value the lowest possible value. This is a critical parameter that was determined using a different approach and independently verifies several types of gamma-ray attenuation parameters that were carefully explored in the previous sections of the current investigation.

Conclusion

The elastic moduli and the ability of gamma radiation shielding as well as transmission factor (TF) of four samples of tungsten bario-phosphate glasses with chemical formula $xBaO\text{-}40WO_3\text{-}(60\text{-}x)P_2O_5$: (x = 10 (S1), 20 (S2), 30 (S3), and 40 (S4) mol%) glasses have been examined. The mentioned aims were achieved by applying Makishima-Mackenzie model, the newly online Phy-X/PSD software, and Monte Carlo simulation code. Our findings revealed that the (V_t) was 0.613, 0.626, 0.612, and 0.643, for S1, S2, S3, and S4, respectively. The (G_t) values were decreased from 62.58 to 55.92 (kJ/cm^3). Values of Young's (E^{MM}) modulus were 76.759 GPa, 75.631 GPa, 71.167 GPa, and 71.966 GPa for S1, S2, S3, and S4, respectively. The (K^{MM}) values were 56.490 GPa, 56.859 GPa, 52.267 GPa, and 55.570 GPa. Poisson's ratio (σ^{MM}) achieved the values 0.273 GPa, 0.278 GPa, 0.273 GPa, and 0.284 GPa. In terms of radiation shielding properties, the S4 sample possessed the highest values of (μ) and (μ_m). However, $(\mu, \mu_m)_{S1} < (\mu, \mu_m)_{S2} < (\mu, \mu_m)_{S3} < (\mu, \mu_m)_{S4}$. Also, The S4 sample possessed the lowest

values of half (HVL), tenth (TVL) value layers, and mean free path (MFP) among all investigated glasses. Therefore, $(HVL, TVL, MFP)_{S4} < (HVL, TVL, MFP)_{S3} < (HVL, TVL, MFP)_{S2} < (HVL, TVL, MFP)_{S1}$. Both ($Z_{eff}$) and ($N_{eff}$) of the proposed glasses have as similar trend. In terms of transmission factor (TF), the sample S4 achieved the minimum values at a thickness of 3 cm. However, the S4 sample showed better radiation shielding properties.

Acknowledgements The authors express their gratitude to Princess Nourah bint Abdulrahman University Researchers Supporting Project number (PNURSP2023R60), Princess Nourah bint Abdulrahman University, Riyadh, Saudi Arabia

Funding Princess Nourah bint Abdulrahman University Researchers Supporting Project number (PNURSP2023R60), Princess Nourah bint Abdulrahman University, Riyadh, Saudi Arabia.

Data availability The data presented in this study are available on request from the corresponding author.

Declarations

The authors declare that this manuscript is original, has not been published before, and is not currently being considered for publication elsewhere.

Informed consent statement Not applicable.

Conflicts of interest The authors declare no conflict of interest.

References

1. Kamiya, K., Ozasa, K., Akiba, S., Niwa, O., Kodama, K., Takamura, N., Zaharieva, E.K., Kimura, Y., Wakeford, R.: Long-term effects of radiation exposure on health. Lancet **386**, 469–478 (2015). https://doi.org/10.1016/S0140-6736(15)61167-9
2. Lee, D.J., Koru-Sengul, T., Hernandez, M.N., Caban-Martinez, A.J., McClure, L.A., Mackinnon, J.A., Kobetz, E.N.: Cancer risk among career male and female Florida firefighters: Evidence from the Florida Firefighter Cancer Registry (1981–2014). Am. J. Ind. Med. **63**, 285–299 (2020). https://doi.org/10.1002/ajim.23086
3. Cardis, E., Vrijheid, M., Blettner, M., Gilbert, E., Hakama, M., Hill, C., Howe, G., Kaldor, J., Muirhead, C.R., Schubauer-Berigan, M., Yoshimura, T., Bermann, F., Cowper, G., Fix, J., Hacker, C., Heinmiller, B., Marshall, M., Thierry-Chef, I., Utterback, D., Ahn, Y.O., Amoros, E., Ashmore, P., Auvinen, A., Bae, J.M., Bernar, J., Biau, A., Combalot, E., Deboodt, P., Diez Sacristan, A., Eklöf, M., Engels, H., Engholm, G., Gulis, G., Habib, R.R., Holan, K., Hyvonen, H., Kerekes, A., Kurtinaitis, J., Malker, H., Martuzzi, M., Mastauskas, A., Monnet, A., Moser, M., Pearce, M.S., Richardson, D.B., Rodriguez-Artalejo, F., Rogel, A., Tardy, H., Telle-Lamberton, M., Turai, I., Usel, M., Veress, K.: The 15-Country Collaborative Study of Cancer Risk among Radiation Workers in the Nuclear Industry: Estimates of Radiation-Related Cancer Risks. Radiat. Res. **167**, 396–416 (2007). https://doi.org/10.1667/RR0553.1
4. Oyar, O., Kişlalioğlu, A.: How protective are the lead aprons we use against ionizing radiation? Diagnostic Interv. Radiol. **18**, 147–152 (2012). https://doi.org/10.4261/1305-3825.DIR.4526-11.1
5. Zakaly, H.M.H., Saudi, H.A., Tekin, H.O., Rashad, M., Issa, S.A.M., Rammah, Y.S., Elazaka, A.I., Hessien, M.M., Ene, A.: Glass fabrication using ceramic and porcelain recycled waste and lithium niobate: physical, structural, optical and nuclear radiation attenuation properties. J. Mater. Res. Technol. **15**, 4074–4085 (2021). https://doi.org/10.1016/j.jmrt.2021.09.138
6. Mansour, A., Abou Hussein, E.M., Saad, E.A., El-Alaily, N.A.: Study of using certain composition of bismuth silicate glass and glass ceramic for gamma radiation processing. J. Nucl. Tech. Appl. Sic. **2**(5), 511–522 (2014)
7. El-Alaily, N.A., Abou Hussein, E.M., Saad, E.A.: Bismuth silicate glass containing heavy metal oxide as a promising radiation shielding material. J. Radiat. Eff. Defects Solids **171**, 11–12 (2016)
8. Ilik, E., Kavaz, E., Kilic, G., Issa, S.A.M., Zakaly, H.M.H., Tekin, H.O.: A closer-look on Copper(II) oxide reinforced Calcium-Borate glasses: Fabrication and multiple experimental assessment on optical, structural, physical, and experimental neutron/gamma shielding properties. Ceram. Int. **48**, 6780–6791 (2022)
9. Zakaly, H.H., Alsaif, N.A.M., Shams, M.S., El-Refaey, A.M., Elsad, R.A., Sadeq, M.S., Rammah, Y.S.: Synthesis, physical, optical characteristics, neutron/γ-rays shielding capacity of newly arsenic glasses: experimental, theoretical, and simulation investigations. Opt. Quant. Electron. **55**, 365 (2023)
10. Norah, A.M., Alsaif, I.O., Olarinoye, Y.S.: Rammah, The role of titania on gamma and neutron attenuation competence of sodium lead borosilicate glasses. J. Aust. Ceram. Soc. **58**, 939–947 (2022). https://doi.org/10.1007/s41779-022-00749-8
11. Alsaif, N.A.M., Olarinoye, I.O., Ahmed, E.M., Rammah, Y.S.: CeO_2-doped bismosiliconate-borotellurite glasses: linear/nonlinear optical properties as well as photon/neutron attenuation effectiveness. J Mater Sci: Mater Electron **33**, 14894–14909 (2022). https://doi.org/10.1007/s10854-022-08407-2
12. Rao, D.: Summary from the SFRP-IRPA workshops "on the reasonableness in the practical implementation of the ALARA principle." Radiat. Prot. Environ. **42**, 187 (2019). https://doi.org/10.4103/rpe.rpe_3_20
13. Needleman, H.: Lead poisoning. Annu. Rev. Med. **55**, 209–222 (2004). https://doi.org/10.1146/annurev.med.55.091902.103653
14. Abouhaswa, A.S., Zakaly, H.M.H., Issa, S.A.M., Pyshkina, M., El-Mallawany, R., Mostafa, M.Y.A.: Lead borate glasses and synergistic impact of lanthanum oxide additive: optical and nuclear radiation shielding behaviors. J. Mater. Sci. Mater. Electron. **31**, 14494–14501 (2020). https://doi.org/10.1007/s10854-020-04009-y
15. Elshami, W., Tekin, H.O., Al-Buriahi, M.S., Hegazy, H.H., Abuzaid, M.M., Issa, S.A.M., Zaid, M.H.M., Sidek, H.A.A., Matori, K.A., Zakaly, H.M.H.: Developed selenium dioxide-based ceramics for advanced shielding applications: Au2O3 impact on nuclear radiation attenuation. Results Phys. **24**, 104099 (2021). https://doi.org/10.1016/j.rinp.2021.104099
16. Deliormanlı, A.M., Ensoylu, M., Issa, S.A.M., Elshami, W., Al-Baradi, A.M., Al-Buriahi, M.S., Tekin, H.O.: WS2/bioactive glass composites: Fabrication, structural, mechanical and radiation attenuation properties. Ceram. Int. **47**, 29739–29747 (2021). https://doi.org/10.1016/j.ceramint.2021.07.146
17. Almisned, G., Elshami, W., Issa, S.A.M., Susoy, G., Zakaly, H.M.H., Algethami, M., Rammah, Y.S., Ene, A., Al-Ghamdi, S.A., Ibraheem, A.A., Tekin, H.O.: Enhancement of gamma-ray shielding properties in cobalt-doped heavy metal borate glasses: The role of lanthanum oxide reinforcement. Materials **14**, 7703 (2021). https://doi.org/10.3390/MA14247703
18. Kilic, G., Ilik, E., Issa, S.A.M., Issa, B., Al-Buriahi, M.S., Issever, U.G., Zakaly, H.M.H., Tekin, H.O.: Ytterbium (III) oxide reinforced novel TeO_2–B_2O_3–V_2O_5 glass system: Synthesis and optical, structural, physical and thermal properties. Ceram. Int. **47**, 18517–18531 (2021). https://doi.org/10.1016/j.ceramint.2021.03.175
19. Saudi, H.A., Zakaly, H.H., Issa, S.M., Tekin, H.O., Hessien, M.M., Rammah, Y.S., Henaish, A.M.A.: Fabrication, FTIR,

physical characteristics and photon shielding efficacy of CeO_2 /sand reinforced borate glasses: Experimental and simulation studies. Radiat. Phys. Chem., 109837 (2021). https://doi.org/10.1016/j.radphyschem.2021.109837
20. Abouhaswa, A.S., El-Agawany, F.I., Ahmed, E.M., Rammah, Y.S.: Optical, magnetic characteristics, and nuclear radiation shielding capacity of newly synthesized barium boro-vanadate glasses: B_2O_3–BaF_2–Na_2O–V_2O_5. Radiat. Phys. Chem. **192**, 109922 (2022). https://doi.org/10.1016/j.radphyschem.2021.109922
21. El-Taher, A., Zakaly, H.M.H., Pyshkina, M., Allam, E.A., El-Sharkawy, R.M., Mahmoud, M.E., Abdel-Rahman, M.A.E.: A comparative study between fluka and microshield modeling calculations to study the radiation-shielding of nanoparticles and plastic waste composites. Zeitschrift Fur Anorg. Und Allg Chemie. **647**, 1083–1090 (2021). https://doi.org/10.1002/zaac.202100062
22. Gökhan Kilic, U.: Gökhan Issever, Erkan Ilik, Synthesis, characterization and crystalline phase studies of TeO_2–Ta_2O_5–ZnO/ZnF_2 oxyfluoride semiconducting glasses. J. Non-Cryst. Solids **527**, 119747 (2020)
23. Issever, U.G., Kilic, G., Ilik, E.: The Impact of CuO on physical, structural, optical and thermal properties of dark VPB semiconducting glasses. Opt. Mater. **116**, 111084 (2021)
24. Kilic, G., Ilik, E., Mahmoud, K.A., El-Mallawany, R., El-Agawany, F.I., Rammah, Y.S.: Novel zinc vanadyl boro-phosphate glasses: ZnO–V_2O_5– P_2O_5–B_2O_3: Physical, thermal, and nuclear radiation shielding properties. Ceram. Int. **46**, 19318–19327 (2020)
25. Issa, S.A.M., Tekin, H.O., Saudi, H.A., Koubisy, M.S.I., Zhukovsky, M., Ali, A.S., Zakaly, H.M.H.: Fabrication of newly developed Tungsten III-oxide glass family: Physical, Structural, Mechanical, radiation shielding effectiveness. Optik (Stuttg) **259**, 169025 (2022). https://doi.org/10.1016/j.ijleo.2022.169025
26. Elias, J.A., Montes, E., Torres-Castro, A., Wiechers, C., Gomez-Solis, C., Vega-Carrillo, H.R., Sosa, M.A., Vallejo, M.A.: Mn, Cu and Cr nanoparticles in $Li_2B_4O_7$ glass: Radiation shielding and optical properties. Radiat. Phys. Chem. **194**, 110037 (2022). https://doi.org/10.1016/j.radphyschem.2022.110037
27. Alqahtani, F.F., Alzuhair, A.Z., Mohamed, S.E., Zahran, H.Y., Alqahtani, M.S., Hussein, K.I., Alshehri, A.M., Yahia, I.S., Reben, M., Yousef, E.S.: Correlation of physical parameters features with optical and radiation shielding properties of heavy glass. Radiat. Phys. Chem. **196**, 110098 (2022). https://doi.org/10.1016/j.radphyschem.2022.110098
28. Singh, S., Kaur, R., Rani, S., Sidhu, B.S.: Physical, structural and nuclear radiation shielding behaviour of xBaO-(0.30-x)MgO-0.10Na_2O-0.10Al_2O_3-0.50B_2O_3 glass matrix. Mater. Chem. Phys. **276**, 125415 (2022). https://doi.org/10.1016/J.MATCHEMPHYS.2021.125415
29. Alzahrani, J.S., Sharma, A., Nazrin, S.N., Alrowaili, Z.A., Al-Buriahi, M.S.: Optical and radiation shielding effectiveness of a newly fabricated WO_3 doped TeO_2–B_2O_3 glass system. Radiat. Phys. Chem. **193**, 109968 (2022). https://doi.org/10.1016/j.radphyschem.2022.109968
30. Alharshan, G.A., Alrowaili, Z.A., Mahmoud, Z.M.M., Olarinoye, I.O., Al-Buriahi, M.S.: Effect of Nb_2O_5 inclusion on the radiation shielding efficiency of TeO_2–ZnO–LiF–NaF glass system. Radiat. Phys. Chem. **196**, 110127 (2022). https://doi.org/10.1016/j.radphyschem.2022.110127
31. Srinivas, B., Bhogi, A., Naresh, P., Chary, M.N., Shareefuddin, M., Alrowaili, Z.A., Mahmoud, Z.M.M., Olarinoye, I.O., Al-Buriahi, M.S.: Fabrication, optical and radiation shielding properties of BaO-TeO2-B2O3-Cr2O3 glass system. Optik (Stuttg) **258**, 168877 (2022). https://doi.org/10.1016/j.ijleo.2022.168877
32. Elazaka, A.I., Zakaly, H.M.H., Issa, S.A.M., Rashad, M., Tekin, H.O., Saudi, H.A., Gillette, V.H., Erguzel, T.T., Mostafa, A.G.: New approach to removal of hazardous Bypass Cement Dust (BCD) from the environment: 20Na_2O-20$BaCl_2$-(60-x)B_2O_3-(x) BCD glass system and Optical, mechanical, structural and nuclear radiation shielding competences. J. Hazard. Mater. **403** (2021). https://doi.org/10.1016/j.jhazmat.2020.123738
33. Purnima, M., Bale, S., Samee, M.A., Ahmmad, S.K., Rahman, S.: AC conductivity and its scaling behavior in MgO–Li_2O–B_2O_3–Bi_2O_3 glasses. J. Phys. Chem. Solids **74**, 189–195 (2013)
34. Purnima, M., Stalin, S., Edukondalu, A., Samee, M.A., Ahmmad, S.K., Rahman, S.: Spectroscopic studies on Li_2O–MgO–Bi_2O_3–B_2O_3 glasses. Chin. J. Phys. **66**, 517–526 (2020)
35. Ahmmad, S.K., Alsaif, N.A.M., Shams, M.S., El-Refaey, A.M., Elsad, R.A., Rammah, Y.S., Sadeq, M.S.: Machine learning density prediction and optical properties of calcium boro-zinc glasses. Opt. Mater. **134**, 113145 (2022)
36. Ahmed, S.A., Rajiya, S., Samee, M.A., Ahmmad, S.K., Jaleeli, K.A.: Density of Bismuth boro zinc glasses using machine learning techniques. J. Inorg. Organomet. Polym. **32**, 941–953 (2022)
37. Kalenda, P., Koudelka, L., Mošner, P., Montagne, L., Revel, B.: Glass-forming ability and the structure of glasses in the BaO-WO3-P2O5 system. J. Non. Cryst. Solids. **541**, 120145 (2020). https://doi.org/10.1016/j.jnoncrysol.2020.120145
38. Makishima, A., Mackenzie, J.D.: Direct calculation of Young's moidulus of glass. J. Non. Cryst. Solids. **12**, 35–45 (1973). https://doi.org/10.1016/0022-3093(73)90053-7
39. Inaba, S., Fujino, S., Morinaga, K.: Young's modulus and compositional parameters of oxide glasses. J. Am. Ceram. Soc. **82**, 3501–3507 (1999). https://doi.org/10.1111/j.1151-2916.1999.tb02272.x
40. Olarinoye, I.O., El-Agawany, F.I., El-Adawy, A., Yousef, E.S., Rammah, Y.S.: Mechanical features, alpha particles, photon, proton, and neutron interaction parameters of TeO_2–V_2O_3–MoO_3 semiconductor glasses. Ceram. Int. **46**, 23134–23144 (2020). https://doi.org/10.1016/j.ceramint.2020.06.093
41. Elkhoshkhany, N., Syala, E., Sayed Yousef, E.: Concentration dependence of the elastic moduli, thermal properties, and non-isothermal kinetic parameters of Yb^{3+} doped multicomponent tellurite glass system. Results Phys. **16**, 102876 (2020). https://doi.org/10.1016/j.rinp.2019.102876
42. Tekin, H.O., Rammah, Y.S., Hessien, M.M., Zakaly, H.M.H., Issa, S.A.M.: Evaluating the optical and gamma-ray protection properties of bismo-tellurite sodium titanium zinc glasses. J. Aust. Ceram. Soc. **1**, 1–16 (2022). https://doi.org/10.1007/s41779-022-00732-3
43. Almatari, M., Agar, O., Altunsoy, E.E., Kilicoglu, O., Sayyed, M.I., Tekin, H.O.: Photon and neutron shielding characteristics of samarium doped lead alumino borate glasses containing barium, lithium and zinc oxides determined at medical diagnostic energies. Results Phys. **12**, 2123–2128 (2019). https://doi.org/10.1016/j.rinp.2019.01.094
44. RSICC Computer Code Collection, MCNPX User's Manual Version 2.4.0. MonteCarlo N-Particle Transport Code System for Multiple and High Energy Applications (2002)
45. Şakar, E., Özpolat, Ö.F., Alım, B., Sayyed, M.I., Kurudirek, M.: Phy-X / PSD: Development of a user friendly online software for calculation of parameters relevant to radiation shielding and dosimetry. Radiat. Phys. Chem. **166**, 108496 (2020). https://doi.org/10.1016/J.RADPHYSCHEM.2019.108496
46. Aktas, B., Yalcin, S., Dogru, K., Uzunoglu, Z., Yilmaz, D.: Structural and radiation shielding properties of chromium oxide doped borosilicate glass. Radiat. Phys. Chem. **156**, 144–149 (2019). https://doi.org/10.1016/J.RADPHYSCHEM.2018.11.012
47. Yalcin, S., Aktas, B., Yilmaz, D.: Radiation shielding properties of Cerium oxide and Erbium oxide doped obsidian glass. Radiat. Phys. Chem. **160**, 83–88 (2019). https://doi.org/10.1016/J.RADPHYSCHEM.2019.03.024
48. Al-Yousef, H.A., Sayyed, M.I., Alotiby, M., Kumar, A., Alghamdi, Y.S., Alotaibi, B.M., Alsaif, N.A.M., Mahmoud, K.A.,

Al-Hadeethi, Y.: Evaluation of optical, and radiation shielding features of New phosphate-based glass system. Optik (Stuttg) **242**, 167220 (2021). https://doi.org/10.1016/J.IJLEO.2021.167220

49. Almuqrin, A.H., Kumar, A., Jecong, J.F.M., Al-Harbi, N., Hannachi, E., Sayyed, M.I.: Li2O-K2O-B2O3-PbO glass system: Optical and gamma-ray shielding investigations. Optik (Stuttg) **247**, 167792 (2021). https://doi.org/10.1016/J.IJLEO.2021.167792
50. Al-Harbi, F.F., Prabhu, N.S., Sayyed, M.I., Almuqrin, A.H., Kumar, A., Kamath, S.D.: Evaluation of structural and gamma ray shielding competence of Li_2O-K_2O-B_2O_3-HMO (HMO = SrO/TeO_2/PbO/Bi_2O_3) glass system. Optik (Stuttg) **248**, 168074 (2021). https://doi.org/10.1016/j.ijleo.2021.168074
51. Bashter, I.I.: Calculation of radiation attenuation coefficients for shielding concretes. Ann. Nucl. Energy. **24**, 1389–1401 (1997). https://doi.org/10.1016/S0306-4549(97)00003-0